Structural analysis of the *Sulfolobus solfataricus* MCM protein N-terminal domain[†]

Wei Liu[1],*, Biagio Pucci[2], Mosè Rossi[2], Francesca M. Pisani[2] and Rudolf Ladenstein[1]

[1]Center of Structural Biochemistry, Karolinska Institutet NOVUM, 141 57 Huddinge, Sweden and [2]Institute of Protein Biochemistry–CNR, Via P. Castellino, 111. 80131-Naples, Italy

ABSTRACT

The Mini-Chromosome Maintenance (MCM) proteins are candidates of replicative DNA helicase in eukarya and archaea. Here we report a 2.8 Å crystal structure of the N-terminal domain (residues 1–268) of the *Sulfolobus solfataricus* MCM (Sso MCM) protein. The structure reveals single-hexameric ring-like architecture, at variance from the protein of *Methanothermobacter thermoautotrophicus* (Mth). Moreover, the central channel in Sso MCM seems significantly narrower than the Mth counterpart, which appears to more favorably accommodate single-stranded DNA than double-stranded DNA, as supported by DNA-binding assays. Structural analysis also highlights the essential role played by the zinc-binding domain in the interaction with nucleic acids and allows us to speculate that the Sso MCM N-ter domain may function as a molecular clamp to grasp the single-stranded DNA passing through the central channel. On this basis possible DNA unwinding mechanisms are discussed.

INTRODUCTION

Mini-Chromosome Maintenance (MCM) proteins form ring-like hexameric complexes which are commonly believed to act as the replicative DNA helicase at the eukaryotic/archaeal DNA replication fork (1,2). The six eukaryotic MCM 2–7 proteins and the archaeal MCM orthologs belong to the AAA+ (*A*TPases with other *a*ssociated cellular *a*ctivities) super-family (3) and contain the highly conserved ATPase sequence box in the central region of their polypeptide chain (4). The intrinsic DNA helicase activity displayed *in vitro* by the MCM 2–7 complex and MCM 4/6/7 subcomplex was found to be weak and not processive (5,6). Conversely, the MCM proteins from the archaea *Methanothermobacter thermoautotrophicus* (Mth MCM) (7,8), *Sulfolobus solfataricus* (Sso MCM) (9) and *Archaeoglobus fulgidus* (Afu MCM) (10) were found to form homo-oligomeric assemblies endowed with a robust 3′–5′ DNA helicase activities *in vitro*. Since archaeal MCM complexes possess a simplified composition and higher structural stability with respect to the eukaryotic counterparts, they have been extensively studied as an excellent model system for structural/functional analyses of these hexameric DNA helicases, which have been recently classified in the helicases super-family 6 (11).

The structures of the Mth MCM complex determined by electron microscopy (EM) have shown various ring-like assemblies, including hexamers (12), heptamers (13), double-hexamers (14), double-heptamers (15) and even filamentous multimers (16). The crystal structure of a N-terminal fragment of Mth MCM (residues 1–286) revealed a double-hexameric architecture with a positively charged central channel wide enough to encircle single-stranded (ss) or double-stranded (ds) DNA (17). However, no structural information has so far been available for other MCM proteins, including Sso MCM, which has become an important subject of biochemical studies in recent years (18–20). In contrast to Mth MCM, the Sso protein assembles as a single hexamer as indicated by analytical gel filtration and glycerol gradient sedimentation analyses, a feature shared by the Afu MCM protein (9,10). Very recently, Sso MCM has been demonstrated to possess a modular organization by limited proteolysis and biochemical characterization of truncated forms of the protein corresponding to the protease-resistant domains (21,22). This analysis has revealed that the Sso MCM C-terminal module comprising the AAA+ and the very C-terminal

domains (AAA + -C-ter, residues 269–686) displays ATPase and DNA-melting activities, whereas the N-terminal module (N-ter, 1–268) retains only a DNA-binding activity.

MATERIALS AND METHODS

Materials

All chemicals were reagent grade. Restriction and modification enzymes were from New England Biolabs. Radioactive nucleotides were purchased from GE Healthcare. Oligonucleotides were synthesized and purified by PRIMM (Milan, Italy). Crystallization reagents were from Hampton Research.

Construction of the plasmid vectors for the expression of the Sso MCM N-ter truncated protein

The construct for the expression of Sso MCM N-ter was generated by a PCR-based approach using the pET29a-SsoMCM vector as the template (9) and the oligonucleotide MCM-Nde-for (5′-AGAAAATATATAGCATATG CAAGGAAATAC-3′) as the forward primer (underlined is the NdeI restriction site) and the oligonucleotide MCM-Eco-rev (5′-ATTGGAATTCCTAGACTTTTTTG TAACATTC-3′) as the reverse primer (the EcoRI restriction site is underlined in the reported sequence). The amplified DNA fragment was subcloned into NdeI/EcoRI-linearized pET29a vector (Novagen) to create the pET29a-SsoMCM-N-ter plasmid. The insert of this plasmid construct was sequenced in order to verify that mutations had not been introduced during PCR.

Purification of the Sso MCM N-ter protein

The SsoMCM N-ter protein was produced in *Escherichia coli* BL21 (DE3) Rosetta cells (Novagen) transformed with the expression vector pET29a-SsoMCM-N-ter. Cultures were grown at 37°C in 4 l of LB medium containing 30 µg/ml kanamycin and 30 µg/ml chloramphenicol. Induction with IPTG starts when the baterial culture reached an $Abs_{600 \, nm}$ of 0.8. Cells were harvested after two hours by centrifugation and the pellet was stored at –20°C until use. The recombinant *E. coli* cell pellet was thawed and re-suspended in buffer A (25 mM Tris–HCl, pH 8.0, 2.5 mM $MgCl_2$) supplemented with a cocktail of protease inhibitors (Sigma). Cells were lysed by two consecutive passages through a French pressure cell apparatus (Aminco Co., Silver Spring, MD, USA) at 2000 p.s.i. The resulting cell extract was centrifuged for 30 min at 30 000 rpm (Beckman) at 10°C. The supernatant was heat-treated at 70°C for 10 min followed by incubation on ice for another 10 min, and then the thermo-precipitated proteins were removed by centrifugation. After adding sodium chloride to a final concentration of 50 mM, the supernatant was filtered and loaded onto a Mono Q HR 10/10 column (GE Healthcare) equilibrated in buffer B (25 mM Tris–HCl, pH 8.5, 2.5 mM $MgCl_2$, 50 mM NaCl). Bound proteins were eluted from the column with a linear gradient of NaCl (0.05–1.0 M). Fractions containing the recombinant protein were pooled. The sample, dialyzed against buffer C (25 mM Tris–HCl, pH 8.0, 2.5 mM $MgCl_2$, 400 mM NaCl, 10% glycerol (v/v)) and concentrated, was subjected to a preparative gel filtration chromatography on a Superdex G 75 HR 16/60 column (GE Healthcare) in buffer C. The recovered sample was concentrated to about 8 mg/ml. Protein concentration was estimated by the Bio-Rad assay (Bio-Rad laboratories) from titration curves made with bovine serum albumin as a standard.

Crystallization and data collection

The concentrated protein was stocked in 25 mM Tris–HCl, pH 8.0, 2.5 mM $MgCl_2$ and 400 mM NaCl. Two crystallization conditions were screened out and later optimized at room temperature using the sitting drop vapor diffusion technique, which resulted in two different crystal forms. Crystals with regular shape of hexagonal prisms were grown with 1.8 M ammonium sulfate in sodium citrate buffer, pH 5.6–6.2, while plate-shaped crystals were obtained under low salt condition in which 20% PEG 3350 was used as the major precipitant with 0.2 M magnesium sulfate in sodium acetate buffer, pH 5.5. Diffraction data for both crystal forms were collected at the beam-lines ID23-1 and BM14, respectively at the ESRF, Grenoble (France). Indexing results showed that they belong to the space groups P1 and C2, respectively.

Structure solution and refinement

The crystal structure in space group C2 was solved by molecular replacement using the program *PHASER* (23). A search model was built from the coordinates of one subunit of Mth MCM (PDB code: 1LTL) (17) by maintaining all identical amino acids but mutating all the others into serine residues. Owing to the substantial movement of domain B and obvious conformational differences in domain A between the two MCM proteins, the main chain of domain A and B had to be manually remodeled. Simulated annealing was done at the intervals of modeling to remove errors and improve density map. Once all amino acids were well-fitted into the electron density, the structure was refined by the program *REFMAC* (24) using TLS refinement approach. The final refined model was later used as the search model for the P1 crystal, in which six protomers were found to form a ring in the asymmetric unit. The same refining protocol using *REFMAC* after simulated annealing was applied on this structure. All data collection and refinement statistics are summarized in Table 1.

DNA band-shift assays

The complementary synthetic oligonucleotides used to prepare the blunt DNA duplex had the following sequence: 5′-TCTACCTGGACGACGACCGGGTATA TAGGGCCCTATATATAGGGCCAGCAGGTCCATC A-3′ (56-mer upper) and 5′-TGATGGACCTGCTGGCC CTATATATAGGGCCCTATATACCCGGTCGTCCA GGTAGA-3′ (56-mer lower). The 56-mer upper oligonucleotide was labeled using T4 polynucleotide kinase and [γ-^{32}P]ATP, as previously described (9). The labeled oligonucleotide was annealed to a 2-fold molar excess of the cold complementary strand (56-mer lower) to prepare

the double-stranded DNA ligand. For the DNA mobility shift assays, 10 µl mixtures were prepared which contained: 200 fmol of [³²P]-labeled DNA in 20 mM Tris–HCl, pH 7.5, 100 mM NaCl, 2 mM EDTA, 0.5 mM MgCl₂, 0.7 mM 2-mercaptoethanol, and the indicated amounts of protein. Following incubation for 10–15 min at room temperature, complexes were separated by electrophoresis through 5% polyacrylamide/bis gels (37.5:1) in 0.5× TBE. Gels were dried down and analyzed by phosphor imaging. The total percentage of protein–DNA complexes for each protein concentration was plotted against the concentration of free protein (as a monomer). Free protein concentration was determined by subtracting the concentration of the bound protein from the total protein concentration, assuming that all

Table 1. Summary of X-ray data collection and refinement

Data collection		
Space group	C2	P1
Cell parameters	a = 193.99 Å, b = 52.24 Å, c = 115.57 Å	a = 53.03 Å, b = 113.75 Å, c = 114.31 Å
	α = 90°, β = 124.15°, γ = 90°	α = 53.03°, β = 82.97°, γ = 86.21°
Resolution range	31.9 – 2.80 Å	49.1 – 3.0 Å
Reflections	443 027/24 102	377 273/40 557
Completeness[a]	99.9%/100%	88.6%/85.2%
$I/\sigma(I)$[a]	21.07/4.35	16.79/2.19
R_{symm}[a]	0.064/0.481	0.041/0.346
Refinement		
Protein subunits	3	6
Missing residues	1–7, 266–268	1–7, 266–268
Water molecules	39	–
R_{work}/R_{free}	0.233/0.283	0.277/0.346
rmsd bond length	0.016 Å	0.020 Å
rmsd bond angle	1.652°	1.804°

[a]Values on both sides of the slash are from the whole data set and the highest resolution shell.
[b]Values separated by slashes are percentage of residues in the core, allowed, general and disallowed regions, respectively.
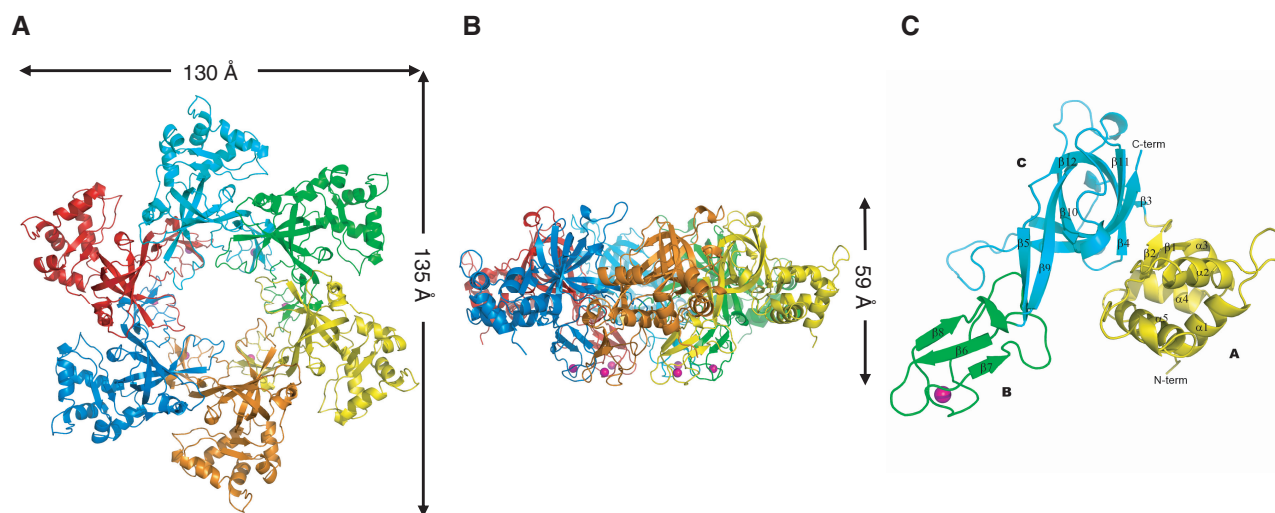
complexes represent bound hexamers. Where saturation was reached, binding data were fit to sigmoidal binding curves by nonlinear least square analysis. The Hill coefficient (n_{app}) and the concentration at the mid-point of the titration curves ($S_{0.5}$) were determined. Experiments were performed in triplicate and the results averaged. The program GraFit (version 3.1) was used for these calculations.

RESULTS

Overall structure

In the crystallization trials, two crystal forms were obtained from completely different conditions; one using high salt but the other bearing low-ionic strength. These crystals belong to the space groups P1 and C2, respectively. The data quality of C2 crystals is better in terms of completeness, I/σ and R-factor (Table 1) due to the sensitivity of the P1 crystal against the cryo-buffer. As a result, the model quality in space group C2 is superior to that in P1, and thus structure descriptions hereafter as well as figure preparation are based on the C2 structure only. Even so, the structures of the Sso MCM N-terminal domain (residues 1–268) in both crystal forms revealed a similar single hexameric ring-like assembly (Figure 1A and B), distinct from the double hexamer of Mth MCM. This architecture agrees well with previous reports showing that the MCM proteins from *Sulfolobus solfataricus* and *Archaeoglobus fulgidus* form single rings in solution (9,10). The protein packs in a similar way in these two space groups, i.e. one hexamer makes loose contacts to another in the head-to-end manner, clearly indicating that Sso MCM N-ter can form stable single hexamers under various conditions, as long as the protein concentration is high enough. As shown in Figure 1A and B, the ring size in the top view is slightly larger than that reported for Mth MCM, although its height equals exactly to one half of the Mth MCM double-hexamer (17).

Figure 1. Overall and subunit structure of the Sso MCM N-terminal domain. Top (**A**) and side (**B**) view of the hexamer forming a single-layered ring. The six subunits are painted with different colors. (**C**) Ribbon model of the subunit structure showing the three distinct domains (A, B and C) rendered in yellow, green and cyan, respectively. The zinc atoms are denoted by magenta spheres.

Subunit structure

The two crystal forms revealed almost identical subunit structures with an rmsd of 1.3 Å based on Cα-atom superimposition. Like Mth MCM, the peptide chain of the Sso MCM N-terminal domain also folds into three distinct domains: A, B and C (Figure 1C). Domain A protrudes out of the ring, endowing the hexamer with a 'snowflake' appearance; domain B contains the zinc-binding motif and domain C provides a large buried area between subunits. The topology of Sso MCM N-ter analyzed by *PDBSUM* (25) is very similar to Mth MCM (17) except for the discontinuity of a β-strand bridging domain B and C. The strand corresponding to β4 in Mth MCM is divided into two shorter strands in Sso MCM, β5 and β6, probably arising from a substantial movement of domain B in comparison with the Mth counterpart (Figure 3B). In addition to the variability of β-strands, two more 3_{10} helices are present in Sso MCM, one located between α5 and β2 in domain A and the other between β10 and β11 (Figure 1C). Two loops display a high degree of flexibility as revealed by weak electron density and higher B-values above the mean level. One of them present in domain A (residues 21–30) extends from the external surface of the hexameric ring, and the other (241–251) forms a loop corresponding to the β-hairpin finger pointing to the hexamer center in Mth MCM (225–228), but is longer and adopts a more extended conformation in Sso MCM.

The central cavity and β-hairpin loop

Similar to Mth MCM, the Sso MCM hexamer contains a unique central channel with an inner surface predominated by positively charged residues, suggesting its physiological role as a DNA-binding surface. The encircled cavity displays a funnel-like contour in the interior of the hexameric ring, with wide opening on its top (diameter of 46 Å) and a much narrower channel close to the bottom (24 Å; Figure 2A). Notably, the encircled channel through the top till the bottom in the Sso hexamer is apparently smaller than that of the Mth protein (Figure 2B). In particular, the narrowest region inside the Sso channel is 17 Å only (Figure 2A), significantly smaller than the value (23 Å) reported for the crystal structure of the Mth MCM N-ter (17). Possible errors from different measurement methods could be ruled out since the same protocol was used in both cases such that all distances were measured from side chain to side chain (17). The narrowest part in the central cavity occurs at the β-hairpin loop (241–251) which connects the last two strands (β11 and β12) in domain C (Figure 1C), and are believed to be crucial for DNA binding (18). These loops are longer than the Mth MCM counterparts due to a five-residue insertion in the Sso MCM primary sequence (Figure 3A) and project further toward the interior encircling a smaller space thereby. Obviously such a narrow hole occurring in the central channel makes it difficult to accommodate dsDNA with a diameter of 23.7 Å in canonical B-form. Recent molecular mechanics studies of DNA translocation have shown that a hole with a minimum diameter of 20 Å is required for dsDNA
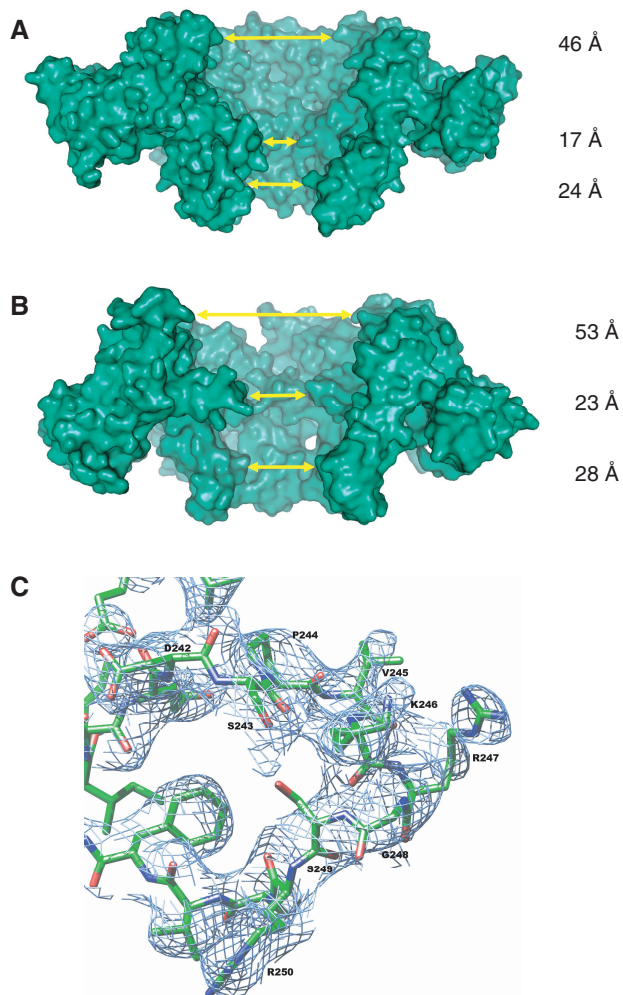

Figure 2. The central cavity and the β-hairpin loop encircling the narrowest space. (**A**) The accessible surface showing the shape and dimension of the cavity interior of the Sso structure, and (**B**), the same representation of the crystal structure of Mth MCM N-ter (17). For clarity, two subunits were taken away from the front. (**C**) Electron density (*2Fo–Fc*) map contoured at 1.0 σ level around the peptide region from residues 241 to 251. The protein atoms are represented in stick model.

to permeate without loosing its structural integrity (26,27). Nonetheless, the flexibility of this β-hairpin loop restricting the narrowest space should be taken into consideration. This region shows increased flexibility indeed compared with other fragments in the current model. The side chains of amino acids on this loop are weakly defined but its main chain atoms fit well into the electron density (Figure 2C), indicating the pore wideness might be somewhat influenced by the structural mobility of the hairpin loops. Even so, from the current model one can still expect that, accommodation of dsDNA requires substantial conformational changes on the hairpin region for significant channel widening and/or considerable distortion of dsDNA as well. In contrast, encircling of ssDNA apparently does not need such big conformational changes on either the protein or the nucleic acid. Based on these considerations, we believe that the Sso
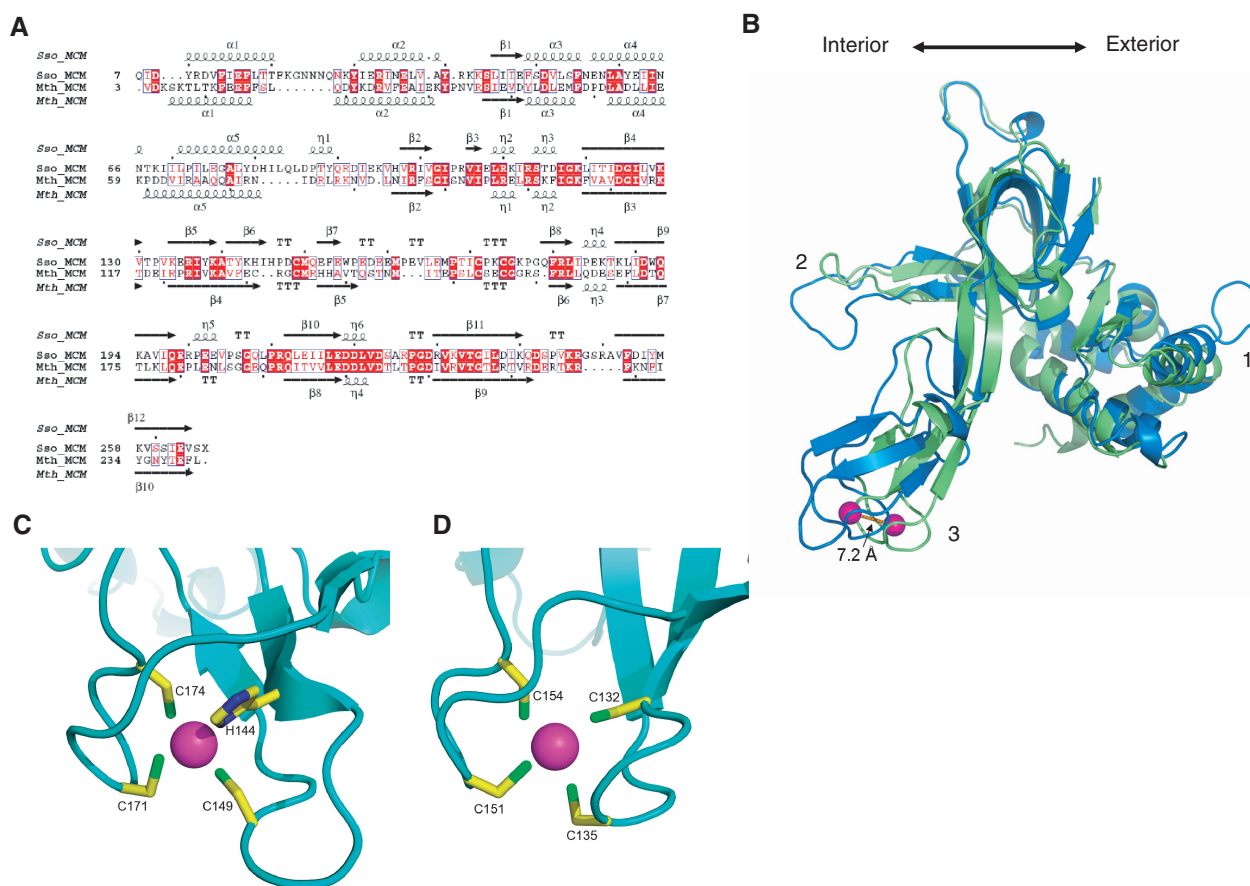
Figure 3. Structural comparison between the Sso and Mth MCM N-terminal domains. (**A**) Structure-based sequence alignment. (**B**) Superimposition of two structures: Sso MCM colored in blue, Mth MCM in green, zinc atoms are represented by magenta spheres. The three regions producing a large rmsd are labeled with numbers. C and D, The zinc-finger motives in Sso (**C**) and Mth (**D**) MCM.

MCM N-ter portion is more suited to encircle ssDNA in terms of energy and steric hindrance under physiological conditions, although dsDNA binding cannot be completely ruled out. Modeling attempts also revealed hints supporting this speculation. Only ssDNA could permeate the central channel without any spatial conflict with protein atoms, but dsDNA inevitably clashes with both main chain and side chain atoms at the narrowest region (data not shown).

Structural comparison with Mth MCM N-ter

As *Sulfolobus* and *Methanothermobacter* belong to Crenarchaea and Euryarchaea, respectively, it would be interesting to compare the structures of their MCM proteins. Structure-based sequence alignment (Figure 3A) and subunit superimposition on *Cα* atoms (Figure 3B) were made to this end. The two proteins share 28% sequence identity and an rmsd of 2.6 Å on main chain overlay. Nevertheless, striking divergence could be seen, mainly occurring in three regions (Figure 3B). First, a loop present in domain A (residues 21–30) protrudes from the outer surface of the Sso MCM hexameric ring, but the equivalent peptide in Mth MCM is much shorter and folds into a tight turn. Given the unknown function of domain A and poor conservation of the amino acid

sequence between residues 21–30 even in Crenarchaea, the significance associated with this protruding loop in Sso MCM is uncertain. Another loop (241–252) present in domain C forms a longer β-hairpin in Sso MCM. As described above, it extends deeper into the central cavity, leading to narrower encircled space for DNA. Conserved basic residues on this loop (K246 and R247) were demonstrated to be crucial in DNA remodeling (18). In addition to these longer loops, the most remarkable feature in the Sso MCM structure was found in the zinc-binding domain, which is described below.

The zinc-binding domain shifts closer to the central channel

All MCM proteins contain a zinc-binding domain within the N-terminal half of their polypeptide chain. Either the C_4 or the HC_3 type has been found in the sequences of the archaeal MCM homologs. Sso MCM contains a non-classical zinc-finger motif with a sequence ($H-X_4-C-X_n-CX_2-C$) divergent from the one ($C-X_2-C-X_n-C-X_2-C$) present in Euryarchaea, like *M. thermoautotrophicus*, *A. fulgidus* or *Pyrococcus abyssi* (Figure 3A) (28). According to a recent structural classification of zinc-finger motives (29), both types belong to the zinc-ribbon super-family due to the occurrence of two knuckles connecting three anti-parallel β-stands and a long disordered loop

(residues 156–178 in Sso MCM). Each knuckle donates two ligands for zinc coordination, arranged in left-handed geometry in both structures (Figure 3C and D). The first knuckle in Sso MCM (Figure 3C), though, is longer than the Mth counterpart (Figure 3D) on which an extra histidine residue (H146) is present. This amino acid is not involved in zinc coordination, but has been identified as a crucial residue in DNA binding (19). Despite common features, the orientation of the zinc-binding motif in Sso MCM diverges obviously from that in Mth MCM (Figure 3B). In the current structure, the zinc atom moves 7.2 Å with respect to that of Mth MCM, leading to poor superimposition between the two structures (Figure 3B). This is why remodeling was required after phasing (see Materials and Methods section). The spatial shift is partially towards the central cavity, which results in considerable shrinkage of the channel bottom from 28 Å of Mth MCM to 24 Å of the Sso structure (Figure 2A and B). Although the biological functions of the zinc-ribbon domains are versatile, they are often found to be involved in protein–DNA (30) or protein–protein interactions (31). The role of the MCM proteins zinc-binding domain has not yet been fully clarified. The Mth MCM N-ter crystal structure shows that the zinc-binding domains are located at the hexamer–hexamer interface, but biochemical studies also suggested that this domain might be involved in DNA binding (19,32). The crystal structure in our study clearly reveals a significant spatial shift of the zinc-binding motif and a narrower outlet for DNA passage. This pronounced structural divergence favors the idea that the zinc-ribbon domain may play a role in DNA binding/remodeling in Sso MCM. In the refined structure, as a matter of fact, some amino acids in that domain inevitably contact the nucleic acid, if DNA, whether ds or ss, is assumed to be encircled in the central channel of Sso MCM.

DNA-binding activity of Sso MCM and its truncated derivatives

In a previous report on the modular organization of Sso MCM, the DNA-binding capability of various truncated forms of this protein were analyzed by electrophoretic mobility shift assays (EMSAs) (22). This analysis revealed that the N-ter module binds a single-stranded 56-mer oligonucleotide with an affinity comparable to the full-sized protein; whereas the AAA + -C-ter derivative binds ssDNA with an affinity greatly reduced and binding saturation was not reached even at a high protein/DNA molar ratio. Here, we investigated the ability of Sso MCM and its truncated forms to bind a 56-bp blunt-ended dsDNA by EMSAs. As shown in Figure 4, the N-ter protein is noticeably impaired
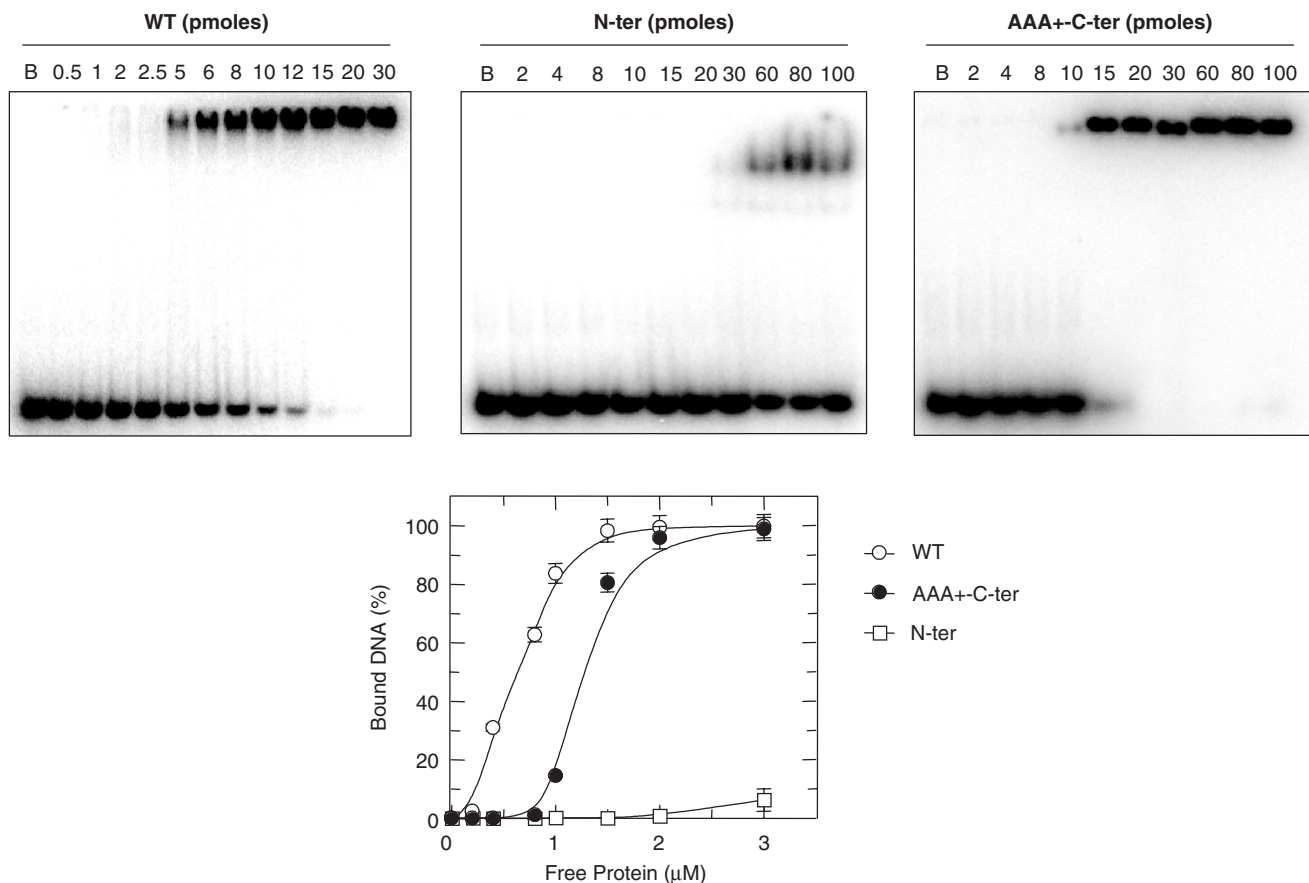

Figure 4. DNA-binding activity of Sso MCM and its truncated forms on blunt dsDNA. Representative EMSAs were carried out with increasing concentrations of each indicated protein using a radio-labeled 56-bp DNA as a ligand. Control mixtures without protein were run on the lanes indicated by B. Plots of the shifted DNA versus the free protein concentration (as a monomer) are shown. Experiments were performed in triplicate and the results averaged. Curves represent best fits to the data points. The error bars on the graphs are the standard error of the mean.

in binding this ligand: a partial shift of the DNA probe was observed only at a very high protein/DNA molar ratio (60 pmol of monomeric protein versus 200 fmol of DNA ligand). On the other hand, the full-sized Sso MCM and the AAA+-C-ter protein are able to bind blunt DNA duplex with comparable higher affinity and the binding curves revealed that these proteins associate to dsDNA in a cooperative manner (Figure 4). This prompted us to fit the binding data to the Hill equations in order to calculate the Hill coefficient (n_{app}) and the $S_{0.5}$ values, the protein concentration at the mid-point of the titration curve, as described in Materials and Methods section. The values of n_{app} obtained for both proteins are much greater than 1 (4 ± 0.2 and 6 ± 1 for the full-sized Sso MCM and the AAA+-C-ter derivative, respectively), clearly indicating cooperative binding to the dsDNA ligand. The $S_{0.5}$ values calculated for the two proteins are comparable (0.51 and 1.2 μM for the full-sized Sso MCM and the AAA+-C-ter derivative, respectively). The simplest interpretation of these results is that at low concentrations Sso MCM is mainly present in solution in a monomeric state with low dsDNA-binding affinity; whereas, at higher protein concentrations the formation of stable hexameric assemblies with higher dsDNA-binding activity is favored.

DISCUSSION

The crystal structure of the Sso MCM N-terminal module reveals a fold similar to the Mth MCM counterpart, but important distinctive features can be observed. First of all, the single-hexamer architecture found in two different crystal forms of Sso MCM is a distinctive feature with respect to the Mth counterpart (17), which undoubtedly corroborates the results of previous biochemical studies (9). Nonetheless, it has been recently reported that highly concentrated samples of the full-length Sso MCM elute from a gel filtration analytical column with a complex broad chromatographic profile compatible with the presence of double-hexameric species (21). This finding is consistent with the hypothesis that the MCM complex is loaded at the replication initiation sites in a transient double-hexameric form. However, *in vivo* biochemical analyses are required in order to establish whether these double-hexameric assemblies are biologically relevant. More strikingly, the Sso MCM N-ter protein seems more likely to encircle ssDNA, since the diameter of its central channel appears to be significantly smaller than that of the Mth protein, particularly at the narrowest region where the β-hairpin loops are located (Figure 2A and B). The possibility of dsDNA binding cannot be completely ruled out, but it would require dramatic conformational changes of the β-hairpin loop, as revealed by structural analysis and modeling attempts. By contrast binding of ssDNA seems more likely since no considerable conformational changes on either protein or the nucleic acid is essentially needed. These considerations are consistent with DNA binding preferences of the Sso MCM truncated forms analyzed by EMSAs. In fact, the N-ter protein displays high affinity for ssDNA (22), but much lower for dsDNA (Figure 4), while the C-ter module

(residues 269–686) shows comparable affinity for dsDNA as the intact protein (Figure 4).

Another distinctive feature of our structure resides in the orientation of the zinc-binding domain. The physiological role played by this domain in the MCM proteins has not yet been clearly elucidated. Structural and biochemical studies on Mth MCM stressed the idea that the zinc-finger motif is involved in hexamer–hexamer contacts (17,33), but some reports revealed that it is involved in efficient interaction with ssDNA (28,32). Given that Sso MCM mainly assembles into single hexamers, it seems unlikely that its zinc-ribbon domain is responsible for hexamer–hexamer interaction. Previous mutational data (19) and the results of our structural analysis both suggest its crucial role in DNA binding/remodeling. The spatial shift towards the channel interior in comparison with Mth MCM enables the Sso MCM zinc-fingers to be closer and form contacts to the encircled DNA. Based on the results of these structural and biochemical studies, we propose that the Sso MCM N-ter portion may function as a molecular clamp for ssDNA with major protein–DNA contacts relying dominantly on both the β-hairpin loop and the zinc-binding motif.

Different possible models were proposed for the helicase activity of the MCM complex (34). The rotary pump (35) model is not applicable to Sso MCM because it is based on the ability of the helicase to encircle dsDNA through the entire length of its central channel. Even the LT-ag model is not appropriate because it envisages that the active helicase has a stable double-hexameric structure (36). Conversely, despite the lack of experimental evidences about its oligomeric state *in vivo*, Sso MCM functions as an active helicase very likely in the form of a single hexameric ring. Recently, a new model has been proposed in which the traditional picture of two replication forks propagating bi-directionally is preserved and the functional helicase unit is a single hexamer that separates the two complementary strands by means of a proteinaceous 'ploughshare' (34). A consistent model for the Sso MCM unwinding mechanism would imply that dsDNA is bound in the AAA+-C-ter central channel, where the two complementary strands are separated in an ATPase-dependent process; the unwound strand with 3′–5′ polarity (the leading strand) would be extruded by the action of the N-ter portion, whereas the other strand (the lagging strand) is expected to loop out from putative lateral channels. Structural studies on SV40 LT-ag (37) and Mth MCM (12,14,15) revealed in both cases the presence of lateral holes on the hexameric wall. These side channels, visible at the border between the N- and C-terminal domains in high-resolution EM structures of Mth MCM (14,15), could be present in the same location even in Sso MCM considering the high structural similarity between these two archaeal proteins. It is interesting to observe that in the crystal structure of Mth and Sso MCM N-ter modules the diameter of the inner channel becomes quite wide on the C-terminus side, consistent with the big central cavity observed between N- and C-terminal domains in the EM images of Mth MCM (15). The encircled space at this region is big enough to accommodate the two melted strands. The proposed model is

consistent with our results on the DNA-binding preferences of the Sso MCM deleted forms (Figure 4) (22). An additional argument in favor of the 'ploughshare' model resides in the finding that either Afu MCM or mouse MCM 4/6/7 complex were reported to bind bubble-containing DNA molecules with high affinity and to protect the ds/ssDNA junctions from nuclease digestion in foot-printing experiments (10,38). Furthermore, it was proposed that DNA strand separation takes place within the Mth MCM central channel by the ATPase-driven coordinated motion of the β-α-β insert in helix-2 and the pre-Sensor 1 β-hairpin (39). Nonetheless, an interesting alternative is represented by the steric-exclusion model, in which the helicase translocates on one DNA strand while the other is physically excluded from the hexameric ring (34). This model was originally proposed for the unwinding mechanism of some bacterial helicases, such as DnaB (40) and the bacteriophage T7 gp4 protein (41), and has been recently reinforced by the crystal structure of the papillomavirus E1 protein bound to ssDNA (42). The 'steric-exclusion' model was proposed for the Sso MCM helicase action on the basis of fluorescence spectroscopy analyses aimed at probing the DNA-binding mechanism of this protein complex (43). The results of our structural analysis are consistent with the steric-exclusion model, although this makes it more difficult to account for the different DNA-binding specificity of the Sso MCM truncated forms. Resolution of the crystal structure of the full-sized Sso MCM hexameric complex bound to DNA appears to be essential in order to elucidate its helicase mechanism.

REFERENCES

1. Grabowski,B. and Kelman,Z. (2003) Archeal DNA replication: eukaryal proteins in a bacterial context. *Annu. Rev. Microbiol.*, **57**, 487–516.
2. Forsburg,S.L. (2004) Eukaryotic MCM proteins: beyond replication initiation. *Microbiol. Mol. Biol. Rev.*, **68**, 109–131.
3. Erzberger,J.P. and Berger,J.M. (2006) Evolutionary relationships and structural mechanisms of AAA+ proteins. *Annu. Rev. Biophys. Biomol. Struct.*, **35**, 93–114.
4. Tye,B.K. (1999) MCM proteins in DNA replication. *Annu. Rev. Biochem.*, **68**, 649–686.
5. Bochman,M.L. and Schwacha,A. (2007) Differences in the single-stranded DNA binding activities of MCM2-7 and MCM467: MCM2 and 5 define a slow ATP-dependent step. *J. Biol. Chem.*, **282**, 33795–33804.
6. Ishimi,Y. (1997) A DNA helicase activity is associated with an MCM4, -6, and -7 protein complex. *J. Biol. Chem.*, **272**, 24508–24513.
7. Kelman,Z., Lee,J.K. and Hurwitz,J. (1999) The single minichromosome maintenance protein of Methanobacterium thermoautotrophicum DeltaH contains DNA helicase activity. *Proc. Natl Acad. Sci. USA*, **96**, 14783–14788.
8. Chong,J.P., Hayashi,M.K., Simon,M.N., Xu,R.M. and Stillman,B. (2000) A double-hexamer archaeal minichromosome maintenance protein is an ATP-dependent DNA helicase. *Proc. Natl Acad. Sci. USA*, **97**, 1530–1535.
9. Carpentieri,F., De Felice,M., De Falco,M., Rossi,M. and Pisani,F.M. (2002) Physical and functional interaction between the mini-chromosome maintenance-like DNA helicase and the single-stranded DNA binding protein from the crenarchaeon Sulfolobus solfataricus. *J. Biol. Chem.*, **277**, 12118–12127.
10. Grainge,I., Scaife,S. and Wigley,D.B. (2003) Biochemical analysis of components of the pre-replication complex of Archaeoglobus fulgidus. *Nucleic Acids Res.*, **31**, 4888–4898.
11. Singleton,M.R., Dillingham,M.S. and Wigley,D.B. (2007) Structure and mechanism of helicases and nucleic acid translocases. *Annu. Rev. Biochem.*, **76**, 23–50.
12. Pape,T., Meka,H., Chen,S., Vicentini,G., van Heel,M. and Onesti,S. (2003) Hexameric ring structure of the full-length archaeal MCM protein complex. *EMBO Rep.*, **4**, 1079–1083.
13. Yu,X., VanLoock,M.S., Poplawski,A., Kelman,Z., Xiang,T., Tye,B.K. and Egelman,E.H. (2002) The Methanobacterium thermoautotrophicum MCM protein can form heptameric rings. *EMBO Rep.*, **3**, 792–797.
14. Gomez-Llorente,Y., Fletcher,R.J., Chen,X.S., Carazo,J.M. and San Martin,C. (2005) Polymorphism and double hexamer structure in the archaeal minichromosome maintenance (MCM) helicase from Methanobacterium thermoautotrophicum. *J. Biol. Chem.*, **280**, 40909–40915.
15. Costa,A., Pape,T., van Heel,M., Brick,P., Patwardhan,A. and Onesti,S. (2006) Structural basis of the Methanothermobacter thermautotrophicus MCM helicase activity. *Nucleic Acids Res.*, **34**, 5829–5838.
16. Chen,Y.J., Yu,X., Kasiviswanathan,R., Shin,J.H., Kelman,Z. and Egelman,E.H. (2005) Structural polymorphism of Methanothermobacter thermautotrophicus MCM. *J. Mol. Biol.*, **346**, 389–394.
17. Fletcher,R.J., Bishop,B.E., Leon,R.P., Sclafani,R.A., Ogata,C.M. and Chen,X.S. (2003) The structure and function of MCM from archaeal M. Thermoautotrophicum. *Nat. Struct. Biol.*, **10**, 160–167.
18. McGeoch,A.T., Trakselis,M.A., Laskey,R.A. and Bell,S.D. (2005) Organization of the archaeal MCM complex on DNA and implications for the helicase mechanism. *Nat. Struct. Mol. Biol.*, **12**, 756–762.
19. Pucci,B., De Felice,M., Rossi,M., Onesti,S. and Pisani,F.M. (2004) Amino acids of the Sulfolobus solfataricus mini-chromosome maintenance-like DNA helicase involved in DNA binding/remodeling. *J. Biol. Chem.*, **279**, 49222–49228.
20. Moreau,M.J., McGeoch,A.T., Lowe,A.R., Itzhaki,L.S. and Bell,S.D. (2007) ATPase site architecture and helicase mechanism of an archaeal MCM. *Mol. Cell.*, **28**, 304–314.
21. Barry,E.R., McGeoch,A.T., Kelman,Z. and Bell,S.D. (2007) Archaeal MCM has separable processivity, substrate choice and helicase domains. *Nucleic Acids Res.*, **35**, 988–998.
22. Pucci,B., De Felice,M., Rocco,M., Esposito,F., De Falco,M., Esposito,L., Rossi,M. and Pisani,F.M. (2007) Modular organization of the Sulfolobus solfataricus mini-chromosome maintenance protein. *J Biol Chem.*, **282**, 12574–12582.
23. McCoy,A.J., Grosse-Kunstleve,R.W., Storoni,L.C. and Read,R.J. (2005) Likelihood-enhanced fast translation functions. *Acta Crystallogr. D Biol. Crystallogr.*, **61**, 458–464.
24. Murshudov,G.N., Vagin,A.A. and Dodson,E.J. (1997) Refinement of macromolecular structures by the maximum-likelihood method. *Acta Crystallogr. D Biol. Crystallogr.*, **53**, 240–255.
25. Laskowski,R.A., Chistyakov,V.V. and Thornton,J.M. (2005) PDBsum more: new summaries and analyses of the known 3D structures of proteins and nucleic acids. *Nucleic Acids Res.*, **33**, D266–D268.
26. Heng,J.B., Aksimentiev,A., Ho,C., Marks,P., Grinkova,Y.V., Sligar,S., Schulten,K. and Timp,G. (2006) The electromechanics of DNA in a synthetic nanopore. *Biophys. J.*, **90**, 1098–1106.
27. Heng,J.B., Aksimentiev,A., Ho,C., Marks,P., Grinkova,Y.V., Sligar,S., Schulten,K. and Timp,G. (2005) Stretching DNA using the electric field in a synthetic nanopore. *Nano Lett.*, **5**, 1883–1888.
28. Poplawski,A., Grabowski,B., Long,S.E. and Kelman,Z. (2001) The zinc finger domain of the archaeal minichromosome maintenance

protein is required for helicase activity. *J. Biol. Chem.*, **276**, 49371–49377.

29. Krishna,S.S., Majumdar,I. and Grishin,N.V. (2003) Structural classification of zinc fingers: survey and summary. *Nucleic Acids Res.*, **31**, 532–550.

30. Viard,T., Cossard,R., Duguet,M. and de La Tour,C.B. (2004) Thermotoga maritima-Escherichia coli chimeric topoisomerases. Answers about involvement of the carboxyl-terminal domain in DNA topoisomerase I-mediated catalysis. *J. Biol. Chem.*, **279**, 30073–30080.

31. Tubon,T.C., Tansey,W.P. and Herr,W. (2004) A nonconserved surface of the TFIIB zinc ribbon domain plays a direct role in RNA polymerase II recruitment. *Mol. Cell. Biol.*, **24**, 2863–2874.

32. Kasiviswanathan,R., Shin,J.H., Melamud,E. and Kelman,Z. (2004) Biochemical characterization of the Methanothermobacter thermautotrophicus minichromosome maintenance (MCM) helicase N-terminal domains. *J. Biol. Chem.*, **279**, 28358–28366.

33. Fletcher,R.J., Shen,J., Gomez-Llorente,Y., Martin,C.S., Carazo,J.M. and Chen,X.S. (2005) Double hexamer disruption and biochemical activities of Methanobacterium thermoautotrophicum MCM. *J. Biol. Chem.*, **280**, 42405–42410.

34. Takahashi,T.S., Wigley,D.B. and Walter,J.C. (2005) Pumps, paradoxes and ploughshares: mechanism of the MCM2-7 DNA helicase. *Trends Biochem. Sci.*, **30**, 437–444.

35. Laskey,R.A. and Madine,M.A. (2003) A rotary pumping model for helicase function of MCM proteins at a distance from replication forks. *EMBO Rep.*, **4**, 26–30.

36. Sclafani,R.A., Fletcher,R.J. and Chen,X.S. (2004) Two heads are better than one: regulation of DNA replication by hexameric helicases. *Genes Dev.*, **18**, 2039–2045.

37. Li,D., Zhao,R., Lilyestrom,W., Gai,D., Zhang,R., DeCaprio,J.A., Fanning,E., Jochimiak,A., Szakonyi,G. and Chen,X.S. (2003) Structure of the replicative helicase of the oncoprotein SV40 large tumour antigen. *Nature*, **423**, 512–518.

38. You,Z. and Masai,H. (2005) DNA binding and helicase actions of mouse MCM4/6/7 helicase. *Nucleic Acids Res.*, **33**, 3033–3047.

39. Jenkinson,E.R. and Chong,J.P. (2006) Minichromosome mainte-nance helicase activity is controlled by N- and C-terminal motifs and requires the ATPase domain helix-2 insert. *Proc. Natl Acad. Sci. USA*, **103**, 7613–7618.

40. Kaplan,D.L. and O'Donnell,M. (2004) Twin DNA pumps of a hexameric helicase provide power to simultaneously melt two duplexes. *Mol. Cell.*, **15**, 453–465.

41. Egelman,E.H., Yu,X., Wild,R., Hingorani,M.M. and Patel,S.S. (1995) Bacteriophage T7 helicase/primase proteins form rings around single-stranded DNA that suggest a general structure for hexameric helicases. *Proc. Natl Acad. Sci. USA*, **92**, 3869–3873.

42. Enemark,E.J. and Joshua-Tor,L. (2006) Mechanism of DNA translocation in a replicative hexameric helicase. *Nature*, **442**, 270–275.

43. Rothenberg,E., Trakselis,M.A., Bell,S.D. and Ha,T. (2007) MCM forked substrate specificity involves dynamic interaction with the 5′-tail. *J. Biol. Chem.*, **282**, 34229–34234.